Journal of Imaging Science and Technology® 57(3): 030401-1–030401-12, 2013.

Linking the Chemistry and Physics of Electronic Charge Transfer in Insulators: Theory and Experiment

Richard P. N. Veregin▲ and Michael S. Hawkins
Xerox Research Centre of Canada, 2660 Speakman Dr., Mississauga, Ontario L5K 2L1, Canada
E-mail: rick.veregin@xerox.com

Qingbin Li, Sergey Gusarov, and Andriy Kovalenko
National Institute for Nanotechnology, 11421 Saskatchewan Drive, Edmonton, Alberta T6G 2M9, Canada

Abstract. *The surface states model is successful in predicting many salient features of charge transfer in insulative materials, which is critical to electrophotography. This article will discuss how the surface chemistry controls the physics and the chemical potentials, and how it fits the surface states model. The interrelationship of acid–base K_a/K_b values of the materials in contact, measured by inverse gas chromatography, the highest occupied molecular orbitals and lowest unoccupied molecular orbitals and their excited states calculated using DFT (density functional theory) quantum mechanical modeling, the chemical potentials measured by the Kelvin method, and triboelectric charging data are studied. It will be shown that a precursor complex of the contacting materials, prior to the charge transfer event, can be calculated by DFT to predict triboelectric charging both qualitatively and quantitatively. This article focuses on polytetrafluoroethylene, Kynar and PMMA polymers, as well as silica, titania, and alumina.* ©*2013 Society for Imaging Science and Technology.*

[DOI: 10.2352/J.ImagingSci.Technol.2013.57.3.030401]

INTRODUCTION

The surface states model[1,2] has been successful in explaining the physics behind charge exchange in insulators, predicting accurately many of the salient features of charging. The weakness of the model is that it is silent on the nature of the surface states responsible for charge exchange, and even the nature of the charge species itself, ions or electrons, as any charged species can fit within the surface states model. The bidirectional Lewis acid–base charge model[3] was introduced to address this issue, to provide a chemical basis for the electron donors and acceptors in an electronic charge exchange mechanism for insulators. Thus, the Lewis acid K_a and Lewis base K_b values, as measured by inverse gas chromatography (IGC), were shown to be predictive of the charging of electrophotographic toner and carrier materials. Charge transfer was shown to be bidirectional between the two surfaces in contact, with electron donation from base sites on the other material to electron acceptance by acid sites. More recently, quantum mechanical (QM) density functional theory (DFT) molecular modeling[4] has been applied to study the electron transfer process between donor and acceptor states in a bimolecular cluster of polytetrafluoroethylene (PTFE) with varying metal oxides. Although the model did not explicitly include the concept of bidirectional charge transfer, the role of the highest occupied molecular orbitals (HOMOs) and lowest occupied molecular orbitals (LUMOs) in charge transfer was explored, including calculations to model the amount of charge transferred.

The current study provides an initial integration of the surface states model, the bidirectional acid–base model, and QM DFT computer modeling of donor and acceptor states, and provides both a qualitative and a quantitative link between all these disparate aspects of charge transfer in insulators.

EXPERIMENT

All calculations were performed with the DMol3 module from the Accelrys Materials Studio 4.2 commercial software package.[5] DFT was used for the study of the surface electronic properties of all models and the coupled toner/carrier complexes. Due to its main advantages of high accuracy at reasonable computational efficiency, the DFT method has been successfully applied to the electronic structure modeling of materials.[6] Recent extensions of the DMol3 density functional method are designed to make electronic structure calculations for local and gradient-dependent functionals, depending on the accuracy needed. In this study, Perdew's 91 generalized gradient approximation (PW91PW91) was employed as the density functional method.[7] It has been reported that geometries optimized using the PW91 density functional are in better agreement with experiment than those from other functionals, such as the widely used BLYP functional.[8,9] For basis sets, a double numerical basis set with d-polarization functions (DND) was used for all calculations.[10] Our experience has shown that the use of DFT requires careful and extensive functional exploration. For different basis set types, it has been reported that DND performs better than a Gaussian-type basis set of the same size, which is 6–31G*. The DND numerical solutions can give highly accurate DFT solutions for the separated atoms limit for molecular and solid calculations.[11]

The initial structure, optimized structure, and electronic properties of adsorbed polymer complexes on the silica

---

▲ IS&T Member.

Received Dec. 14, 2012; accepted for publication Jul. 15, 2013; published online May 1, 2013. Associate Editor: Hiroyuki Kawamoto.
1062-3701/2013/57(3)/030401/12/$20.00

were studied. The geometry optimization convergence was achieved when the energy, gradient, and displacement were lower than 2×10^{-5} Ha, 4×10^{-3} Ha/Å, and 5×10^{-3} Å, respectively. The calculations of HOMO–LUMO orbitals have been performed to understand the direction of charge transfer of the above models and to identify the most essential factors that could affect electron transfer in these complex models. To further explore the reverse gap and the forward gap of charge transfer, the excited orbitals for the above systems were studied. Generally, 10 levels of unoccupied orbitals (to $m+9$) and 10 levels of occupied orbitals (to $n-9$) were calculated. The lowest energy gaps for both forward electron transfer and reverse electron transfer were collected from this set of twenty orbitals.

For all polymers, a trimer was used to represent the polymer. To distinguish the possible effect of the functional group orientation three functional groups were aligned in the structure to co-ordinate to the same side of the other material in contact. For amorphous silicon dioxide fumed silica, such as that from Degussa used in experimental studies,[12] to mimic the surface hydroxyl groups a one layer cylinder-like model was used to design the native silica (silica free of any surface treatment) with the formula $Si_{12}O_{32}H_{16}$. In this model, all silicon atoms were in tetrahedral geometry and connected by oxygen. The edge of this cylinder was terminated by two hydroxyl groups to represent the geminal silanols ($Si(OH)_2$), which are typical on the (100) surface of β-cristobalite, identified experimentally on the amorphous silica surface as one of the two types of surface hydroxyl groups.[13–15] It was reported that this crystalline phase of silica has a density and refractive index closest to those of amorphous silicon dioxide fumed silica from Degussa.[16–18] The arrangement of this cluster model can sustain two types of silicon atom. The center four silicon atoms are connected by Si–O–Si bonds in a tetrahedral structure to represent the non-hydroxylated surface, whereas all of the eight surrounding silicon atoms have geminal silanols to represent the hydroxylated surface. This methodology was also used to build the alumina and titania models. The Degussa alumina is γ-Al_2O_3, which is in the δ-group structure, with all O ions in CCS packing, and octahedral and tetrahedral lattice vacancies occupied by Al ions (spinel-like structure).[19] P25 titanium oxide from Degussa is 70% anatase and 30% rutile. OH groups on the surface enable favorable six-fold co-ordination.[19]

For measurement of the polarity of charge, pairs of powders were mixed, such that one of the powders was toner sized or smaller (<10 μm) and one of the powders was carrier sized (>20 μm). In one set of experiments Kynar or PMMA was coated onto a 35 μm ferrite core as the carrier, which was mixed pairwise with non-surface treated native oxide additives (Evonik Degussa A300, P25 and aluminum oxide C), or 3 μm Lubron^{TM} L2 PTFE from Daikin Industries. Since the different materials are of varying size and density, an approximate correction for these effects was incorporated into the test, to correct the loadings to similar area coverage of the carrier—so as not to overload the carrier with the test material. Thus the oxides were tested at 0.2 pph, the PMMA particles at 5 pph, and the PTFE at 10 pph, all with respect to the carrier at 100 g. Note that these measurements are only used to assess the sign of the tribo charge, not to obtain quantitative numbers, so the correction for surface area does not need to be accurate, only good enough so that an unequivocal negative or positive charge can be assigned. All samples were then conditioned overnight at 21°C and 10% RH, dry conditions preferred to avoid any effects from water, then charged for 2 min (a short time to reduce any aging effect) in a Turbula mixer. Charge was measured by blow-off with a 15 μm mesh screen. A large PTFE particle, the coarse fraction (>45 μm) from the jet sieving of microFlon 124T4 from Shamrock Technologies Inc., was also utilized as a “carrier” particle in a similar way, measuring charge by blow-off of metal oxide particles silica, titania and alumina at 0.45 pph with 3 g of PTFE “carrier”, reduced due to the small amount of PTFE left after fractioning.

RESULTS AND DISCUSSION

Charge transfer complexes: density functional theory QM modeling

In the surface states model,[1] the difference in chemical potential between insulator surfaces in contact drives the charge transfer, balanced against the surface potential difference due to the charge separation between the two surfaces. When the two fields match, charge transfer stops. Previous work[3] showed that the chemical potential difference arises from a bidirectional charge transfer, both from Lewis base donor sites on surface A to Lewis acid acceptor sites on surface B, and donor sites on surface B to acceptor sites on surface A. The net charge transfer is thus dependent on the difference in energy between these two different charge transfer processes. That difference in energy in turn is the difference in the work functions, or chemical potentials, of the two materials, the contact potential difference, as shown in Figure 1. The quantitative relationships between all these quantities can be readily derived as shown previously[2,3]; the results are shown in Eqs. (1) and (2). One key point is that this model as developed to date[3] applies only to the high density of surface states limit, which means that the observed charging depends on the work function only and not on the density of states. The effective work function of a surface, ϕ_s, will be a simple average over the chemical potential of the acid sites for that surface, ϕ_{as}, and the chemical potential of the basic sites, ϕ_{bs},

$$\phi_s = (\phi_{as} + \phi_{bs})/2. \tag{1}$$

From the high density of states charging model, at a steady state charge value,[1,2]

$$\text{Toner } q/m = (A/2)[(\phi_{ac} + \phi_{bc}) - (\phi_{at} + \phi_{bt})]. \tag{2}$$

Here, the chemical potentials for the two surfaces, ϕ_s, are ϕ_t for the toner and ϕ_c for the carrier: ϕ_{at} for acidic toner sites, ϕ_{bc} for basic carrier sites, ϕ_{bt} for basic toner sites, and ϕ_{ac} for acidic carrier sites. The exact form for the A factor

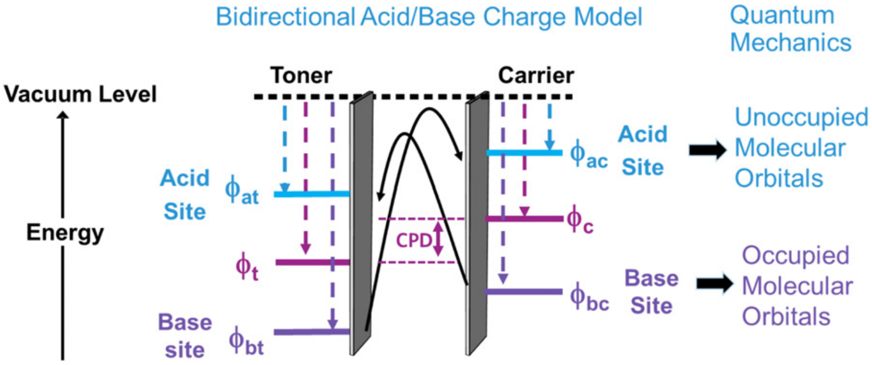

Figure 1. Relationship between acid/base sites in the bidirectional charging model and work functions, chemical potentials, and QM derived frontier molecular orbitals.

depends on the calculation of the electric field: a simple form is $A = 3(\varepsilon_0/d)/(RC_t\rho_c + r\rho_c)$, where d is the tunneling distance, R is the carrier radius, r is the toner radius, ρ_c is the carrier density, ρ_t is the toner density, and C_t is the toner concentration.[1] The A term here is an alternative form to the A_0 of Ref. 1 but with the effect of the geometry on the electric field included. How A_0 and thus A are calculated depends on the how the electric field is calculated and what other assumptions are made.[1,2] Eq. (2) does not limit how A may be calculated. A is of course only a constant at a steady state charge where the geometry and conditions of charging, including mixing intensity and time, are fixed. Note that this model implies that the average work function for a *pure* material does not correspond to an existing physical state. Only the work functions for individual acid sites and the basic sites in an insulative material correspond to actual surface states. Thus the observed work function is only an average over the work functions of the individual acid and base sites in the pure material. It is important to understand that Eqs. (1) and (2) relate to a pure material that has both acid and base sites situated together at the molecular level such that on contact the charge can transfer in both directions between surfaces. Thus there is no weighting factor for the averaging of these work functions, as the dependences of the two donor and acceptor states being accessible at the surface are identical. However, over the whole surface we will have different configurations with different ϕ_s and different probabilities that they are on the surface. Therefore, in that case, we do need to sum over the probability that a particular configuration i is at the surface with a particular ϕ_{si}, so overall $\phi_s = \Sigma p_i\phi_{si}$. Here, p_i is the probability of that surface being accessible to transfer charge, as previously shown for the surface states model.[1,2] For simplicity of presentation this will be ignored in writing the equations in this article. Finally, note that since the contact potential difference (CPD) and work function measurements and charging discussed herein are always taken over a macroscopic area, in practice experimentally all we can measure is $\Sigma p_i\phi_{si}$ over some macroscopic surface area, which at minimum is defined by the contact area in one contact, but in fact generally is much larger depending on the measurement. However, for the modeling all that we can calculate is ϕ_{si} for a selection of configurations since there is no way currently of calculating these surface probabilities. As will be seen, it is remarkable given these fundamental differences that we can use the simple modeling concept to correctly predict charge and work functions, although we will also show some situations where the surface probability for a particular configuration appears to be contributing to the observed charge when compared to that from the modeling.

Finally, the CPD, the difference in work functions, or more properly in the case of insulators, the difference in chemical potentials, is[2]

$$CPD = [(\phi_{ac} + \phi_{bc}) - (\phi_{at} + \phi_{bt})]. \tag{3}$$

In that previous work,[2,3] it was also shown that these ϕ_s values could be related to the surface K_a and K_b acid and base parameters, which can be measured by IGC, and which respectively represent the surface Lewis acidity (the ability to accept an electron), and the surface Lewis basicity (the ability to donate an electron).[20] Thus by a measurement of the surface properties by IGC, the chemical potentials, ϕ_s, were predicted to be linearly related to the ratio of the acid and base parameters for the surface,

$$\phi_s = 1/2\phi^o + 1/2kT\ln(K_a/K_b). \tag{4}$$

Here, ϕ^o is a reference state relating the chemical potentials to the work functions and k is the Boltzmann constant in eV/molecule. A plot of ϕ_s versus $\ln(K_a/K_b)$ provided an excellent fit to the experiment data for a series of metal oxide toner additives (silica, titania, and alumina) as shown Figure 6 in Reference 3, giving

$$\phi_s = 0.50\ln(K_a/K_b) + 4.41\text{ eV}. \tag{5}$$

While the fit was excellent, the predicted slope from Eq. (5) is $kT/2 = 0.013$ eV, compared to the observed value of 0.50 eV. As discussed previously,[3] one possible reason is that the IGC acid–base interactions clearly represent a fractional electron transfer from the donor to the acceptor, and thus might not fully reflect the work functions of the donor and acceptor that are involved in triboelectric charge transfer. There is another possible explanation, in that the derivation of Eq. (4) assumes that the electron transfer is thermally excited. However, for

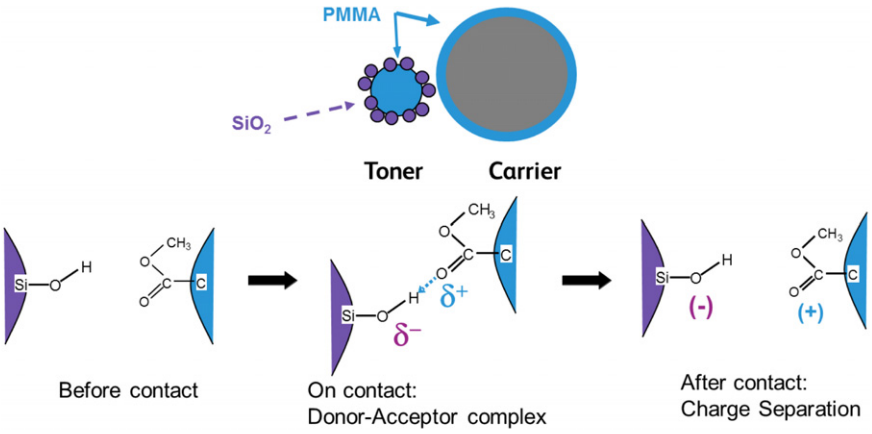

Figure 2. A conceptual model of a donor–acceptor complex and how it leads to charge transfer.

charge transfer by triboelectrification we propose that this is likely not the case, as kT is so much smaller than the energy gaps between donors and acceptors, which are multiple eV, as we shall show shortly. Thus it does seem unlikely that a thermal process could drive the triboelectric charge transfer. Instead, we propose that the electron transfer is activated by the collisional energy, in which case the value of 0.5 in Eq. (5) would then represent that larger energy of activation.

Similarly, the bidirectional charge model[3] expresses toner charge based on the acid and base parameters of the toner and carrier,

$$\text{Toner } q/m = -(A/2)kT[\ln(K_{at}/K_{bt}) - \ln(K_{ac}/K_{bc})]. \quad (6)$$

Equation (6) predicts that toner q/m for a fixed carrier is linear with $\ln(K_{at}/K_{bt})$, with slope $-AkT/2$. Negative charge increases with increasing toner acid-to-base ratio, and charge is zero if the carrier and toner acid-to-base ratios are equal, $K_{at}/K_{bt} = K_{ac}/K_{bc}$. Experimental data for silica, alumina, and titania metal oxide surface additives charging with PMMA have been shown to support the model very well, showing the expected dependence on $\ln(K_{at}/K_{bt})$, and the expected point of zero charge when the acid-to-base ratios match.[3] Further experimental support for the model for a range of toners and carriers has also been published.[21]

Based on this model of acid–base interactions we had proposed a model of what the actual charge transfer event might look like at the molecular level.[22] We proposed that when two surfaces contact, using the example of a silica surface with SiOH groups and a PMMA polymer with ester groups, they form a charge transfer precursor complex in which the acid and base groups of these two surfaces interact. Thus, in Figure 2 a silica surface acid group interacts with a PMMA basic carbonyl group, a complex that is known to exist in the solid state.[23] A key concept here is that there must be something about this precursor state that enables charge transfer, otherwise charge transfer would not occur when the molecules separate. Of course, there would also be a comparable precursor complex where the base site of the silica interacts with the acid site of the PMMA: since both surfaces have acid and base sites, charge transfer is possible in both directions. Both precursor complexes would then contribute to the net charge transfer, as described by the bidirectional charge model for charge exchange.[3] Finally, it is clear that in actual triboelectric charging the collisions or rubbing of two surfaces would tend to be random in nature, unless there is some preferential orientation at the surfaces of the materials. For silica there is a preferential orientation, as the surface is decorated by hydroxyl groups. For a polymer like PMMA, the surface could have many different orientations, and thus any study of charge transfer would necessarily have to understand the effect of different PMMA surface configurations/orientations on the charge transfer complex.

QM can potentially fill in the missing links by studying the nature of the charge transfer complex that enables charge transfer, and identifying the actual donor and acceptor sites that are responsible for the charging process. Nikitina[4] used *ab initio* DFT and time-dependent DFT to study the charge transfer event between PTFE and metal oxides. Briefly, they calculated the lowest energy configuration of the PTFE–oxide charge transfer pair, along with the associated HOMO and LUMO energies and the work function, through to a non-equilibrium excited state, then used time-dependent density functional theory (TDDFT) to an equilibrated final state, where they calculated partial electron densities transferred in the complexes, which they then related generally to charge exchange and the triboelectric series. There was no actual comparison to any specific charging data. Thus they did use QM methods to identify the HOMO and LUMO locations on the molecules and how they might contribute to the charge transfer; however, they did not specifically discuss the chemical nature of these sites.

In the current work we use density functional theory (DFT) quantum mechanical (QM) modeling to further developer this idea of the charge pair that develops on contact. The approach in this study is similar in some ways to Nikitina, but focuses only on the precursor charge transfer complex that develops when materials come into contact, the complex that enables the charge transfer event. As with Nikitina we look at the HOMO and LUMO sites and their energies. We also explore the fit of the QM modeling

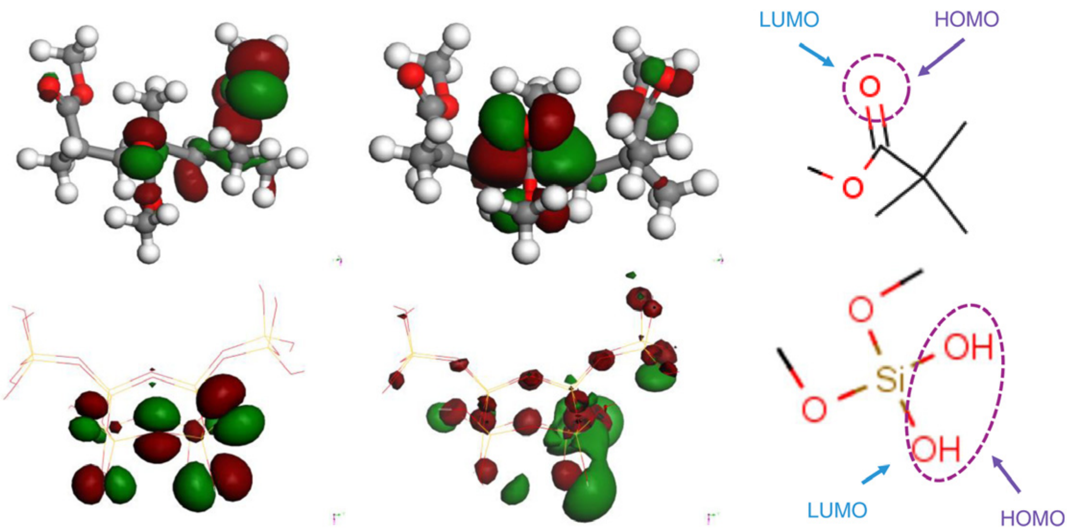

Figure 3. HOMOs and LUMOs for isolated clusters. Top row: PMMA clusters; bottom row: silica clusters. Left: HOMO orbital locations; right: LUMO orbital locations.

within the framework of the bidirectional acid–base charging model, looking at charge transfer in both directions, the effects of the configuration of the charge transfer complex, and the effect of excited states, none of which were included in Nikitina's study. We also extend the work to a number of different polymers as well as metal oxides.

In the first step of our QM modeling, HOMO and LUMO frontier molecular orbitals are calculated for isolated PMMA and oxide molecules; the example with silica is shown in Figure 3. Although it will be the HOMOs and LUMOs in the charge precursor complex that control the charge exchange, we look at the HOMOs and LUMOs of the isolated clusters first to understand the relationship of the isolated HOMOs and LUMOs compared to the precursor complex HOMOs and LUMOs. As shown in Fig. 3, in the isolated PMMA cluster both the HOMO and the LUMO are located on the carbonyl oxygen, while in the isolated silica cluster both are located on the silanol groups. In both cases the HOMO and LUMO are substantially located on the most polarized bonds in the molecules.

We assume that charge transfer occurs with a collision of the two surfaces, which in our QM modeling here is described by the two clusters coming into contact. That contact must provide sufficient energy to enable charge transfer from the HOMO on the donor molecule in the precursor complex, to the LUMO on the acceptor molecule on the complex, as shown in Fig. 1. We will show that these gaps are multiple eV. While electron tunneling charge transfer due to thermally activated processes is well known, the energy gaps are much smaller.[24] Thus it would appear that the collision of the surfaces must provide the bulk of the energy for the charge transfer, if the thermal energy is insufficient. In support of the importance of the energy of the collision of the two surfaces, it has been shown that the charge transferred does depend linearly on the frictional energy dissipated between two surfaces.[25] This would suggest that the energy supplied by the collision (in this case the frictional rubbing of the asperities) is important to triboelectrification. Of course, the contact area will also increase with the collisional energy; however, since the charge density on the surfaces is only one charge for every 10^4 nm^2 at the most in triboelectrification, it seems unlikely that the contact surface area could be a limiting factor. Also, for soft materials such as polymers the required force to level asperities to provide the required contact area for charge transfer is not large, of the order of a kg/cm^2.[26] The frictional energy supplied in reference 25 was 1 mJ/cm^2, which would be over 10 eV per surface bond if all of the energy was absorbed by the surface layer, so of the right order of magnitude to support electron transfer. Indeed, collisional activation processes are well known in mass spectroscopy: when two molecules collide in the gas phase the energy can be sufficient to break the bond and fragment the molecule. This is known as CID, or collisional induced dissociation.[27] More recently it has been shown that molecular collisions with surfaces can also generate sufficient energy to fragment molecules: this process is known as SID, surface-induced dissociation.[28]

The energy available in a typical electrophotographic charging collision was estimated by taking the kinetic energy of a carrier and a toner particle in collision. It was assumed that all the kinetic energy would in some way be imparted to the surface layer of the atoms, ultimately partly adsorbed as heat (energetic motion of the atoms) and partly released back as kinetic energy as the surfaces relax back after the collision. In any event, all that energy is imparted to the surface in contact. Assuming a generous contact area of 1 μm^2 for a toner carrier contact (given that the toner particle will conform somewhat on contact) and that the impact is uniform shows that as much as 10 eV could be imparted to a surface chemical bond. As we will see, this is more than sufficient to overcome the electron transfer gaps of 2.5 to about 6.5 eV that are calculated by our QM modeling. In addition, since triboelectrification involves very few actual charges, only a fraction of the collisions need

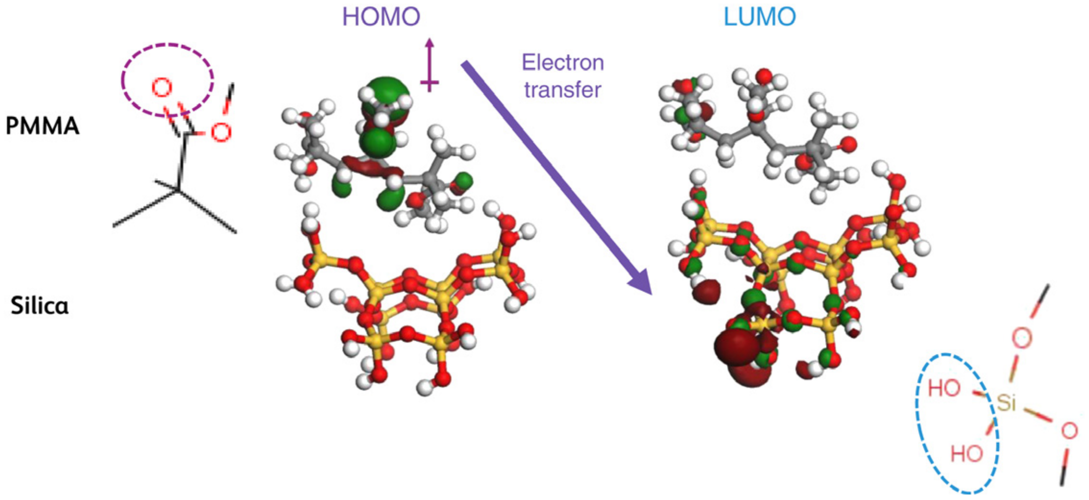

Figure 4. PMMA–silica complex with alkyl groups of PMMA facing silica hydroxyls showing forward charge transfer HOMO and LUMO.

to generate the required energy for charge transfer. Thus, these rough calculations show that the collisional energy could be sufficient to explain the charge transfer processes described here. It should be pointed out that even apparently gentle contacts could provide similar high energies: while the contact is slow and thus low kinetic energy, the contact area can be in the nanometer range as the two surfaces will not conform in such a low energy collision.

One further key point with regard to these collisions is that they will occur at random orientations and are energetic compared to conformational energies. Thus the preferred orientations in collisions should only be those built into the surfaces, such as surface OH groups on metal oxides. Then there is no reason to assume that the lowest energy conformation is the lowest energy for charge transfer, an assumption that was previously made.

Our DFT calculations show that two key orientations of the precursor charge complex are important: those where the polymer dipole either points away from or toward the oxide surface, which for the molecules studied here is equivalent to saying where the HOMO or LUMO on the polymer either points toward or away from the oxide surface. For both of these orientations, energy was minimized and the LUMO and HOMO calculated. In addition, excited states were calculated as well, to be discussed later.

Since the bidirectional charge model[3] shows that charge can transfer in either direction on contact, we will need to identify both of these processes. For the example of PMMA with silica, experiment shows that charge transfers from PMMA to silica, providing negative charge to the silica, positive charge to the PMMA. We will call this the forward charge transfer direction, from the HOMO donor on the PMMA to the LUMO acceptor on the silica. The orientation of the precursor complex that leads to this charge transfer is shown in Figure 4. It corresponds to the PMMA carbonyl dipole pointing *away* from the silica. As we will show later, charge transfer in the reverse direction has a larger energy gap, and thus is less favorable, although it still occurs and is important to the net charge transferred. The HOMO and LUMO molecular orbitals (MOs) for the PMMA–silica complex are also shown in Fig. 4. As with the isolated molecules, the HOMO of the precursor complex, which is on the PMMA, is located on the carbonyl group, while the complex LUMO, which is on the silica, is located on the silanol groups. Thus, the predominant localizations of the HOMO and LUMO are similar in the isolated clusters and in the precursor complex.

The relationship between energy levels for the molecular orbitals in isolated molecules and in the charge transfer complex is shown in Figure 5. For the isolated clusters only the HOMO and LUMO were calculated, while in the precursor complex, the excited states were also calculated. In addition to the lowest energy forward charge transfer, from the HOMO on PMMA to the LUMO on silica, Fig. 5 shows the reverse charge transfer, which corresponds to electron donation from the HOMO−6 excited state of silica to the LUMO+1 of PMMA. As the LUMO+1 and HOMO−6 are excited states of the HOMO and LUMO, the energy gap is larger for the reverse charge transfer than for the forward charge transfer. Thus, the QM modeling predicts that the net effect of the bidirectional charge transfer is a negative charge on the silica and a positive charge on the PMMA, as observed. Two further key general points can be made. It is clearly necessary to consider excited states; without that consideration we would not see the bidirectional nature of the charge transfer in this case. Also note that the HOMO to LUMO energy gap is changed only slightly between isolated molecules and the precursor charge transfer complex; this small change is due to intermolecular orbital overlap. Similarly for the reverse charge transfer, the donor site in the complex, the HOMO−6, corresponds closely in energy to the HOMO on the isolated silica cluster, while the acceptor site in the complex, the LUMO+1 on PMMA, is close in energy to the LUMO on the isolated PMMA cluster, though reduced in energy somewhat. While it is not known at this point whether the close correspondence of the LUMO and HOMO energy levels for the isolated clusters and the precursor charge transfer complex is general

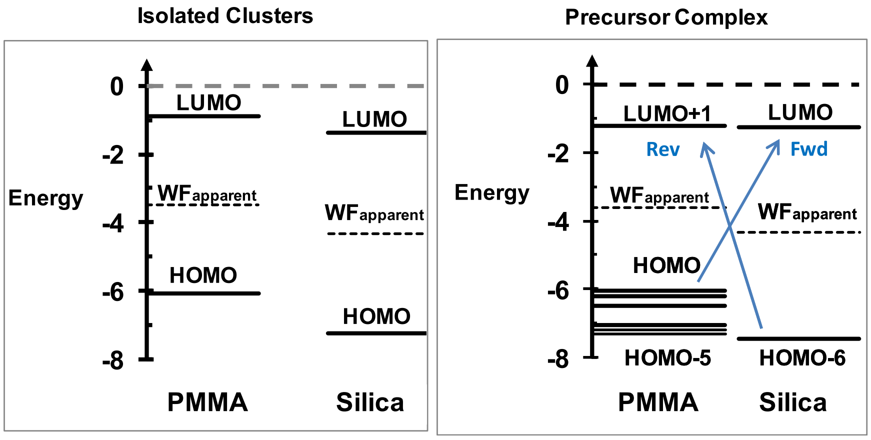

Figure 5. Energy level diagram for molecular orbitals, and relationship to Lewis acid–base parameters for (a) isolated PMMA and silica and (b) the PMMA–silica charge transfer complex. Excited states are not shown for the isolated case.

for triboelectric charge exchange, it needs to be recognized that a self-consistent triboelectric series depends on the difference being small. If the energy difference were large between these states for charge transfer, then the position of a material in the triboelectric series could change dramatically depending on the pairing of materials, and no general tribo series could exist. On the other hand, specific pairwise interactions could explain why sometimes material pairs do not behave as expected based on a strict adherence to the triboelectric series. Thus, a series of materials that adheres strongly to a triboelectric series for all pairwise combinations must have energy levels that are not strongly affected by the intermolecular overlap in the complex. On the other hand, deviations from a strict triboelectric series may be a result of strong intermolecular overlap, or result from the well known effects of surface contamination and physical material transfer.

As mentioned above, two different orientations have been found to be generally useful in understanding the charge transfer properties, one where the carbonyl group faces the oxide, and one where the carbonyl group faces away from the oxide so that the polymer alkyl groups face the oxide. The HOMOs and LUMOs of charge transfer complexes for different oxides with PMMA are shown in Figure 6. Here we make use of the concept of Fukui functions, f, which are defined as the change in electron density when there is an infinitesimal change in the number of electrons. Electron acceptance in a molecule tends to occur where f^+ is large, where the molecule is best able to stabilize an electron. In chemical reactions, these sites are susceptible to nucleophilic attack. Electron donation in a molecule tends to occur where f^- is large, where the molecule is destabilized the least by removal of an electron. In chemical reactions, these sites are susceptible to electrophilic attack. Thus, the Fukui functions are utilized in DFT as important indicators of regioselectivity in electron transfer dominated reactions.[29] As an example we use the electrophilic f^- and nucleophilic f^+ maxima of PMMA to predict the molecular locations of electron donation and acceptance, respectively. The f^+ orientation of PMMA thus has the nucleophilic side facing the silica (the methylene alkyl groups), while the f^- orientation has the electrophilic side of the PMMA cluster, the carbonyl groups, facing the silica. Figure 6 shows the charge transfer precursor complexes for both orientations of the PMMA with silica, alumina, and titania, as well as the most favorable direction for electron transfer with the lowest energy gap. Table I shows the DFT calculated energy gaps for these transfer processes, for both orientations, and for electron transfer from the PMMA to the oxide and from the oxide to the PMMA. In all cases, the f^+ orientation results in the lowest electron transfer gap from the PMMA to the oxide. In other words, when the electron accepting part of the PMMA molecule is facing the oxide, the energy gap is lower for transferring the electron from the PMMA to the oxide. For the f^- orientation of the PMMA toward the oxide, the energy gap is slightly favored for electron transfer from the PMMA to silica, and strongly favored for titania, while for alumina, electron transfer to the PMMA is favored. In general the f^- orientation is more favorable than the f^+ orientation for electron transfer to the PMMA and the f^+ orientation is more favorable for the electron transfer from the PMMA. This seems somewhat counterintuitive, but consideration of the energy levels of the isolated clusters in Fig. 4 suggests why this might be the case for these materials. PMMA has the highest HOMO, and thus is the best donor. Silica has the lowest LUMO, and is the best acceptor. When the surface dipoles of PMMA and silica are pointed away from each other, PMMA f^+ toward silica, the net dipole at the surface is relatively low, and there is nothing to change this preference: the PMMA HOMO and silica LUMO are energetically unperturbed. However, when the surface dipoles of PMMA and silica point in the same direction, PMMA f^- toward the silica, the net dipole at the interface is into the silica, which raises the energy of the HOMO and lowers the energy of the LUMO on PMMA.

Overall, the Fukui functions and the energy gaps predict that silica and titania will charge negative, because both orientations favor electron transfer from PMMA to silica, while with alumina each charge transfer direction is favored in one orientation. Thus, for alumina the two charging

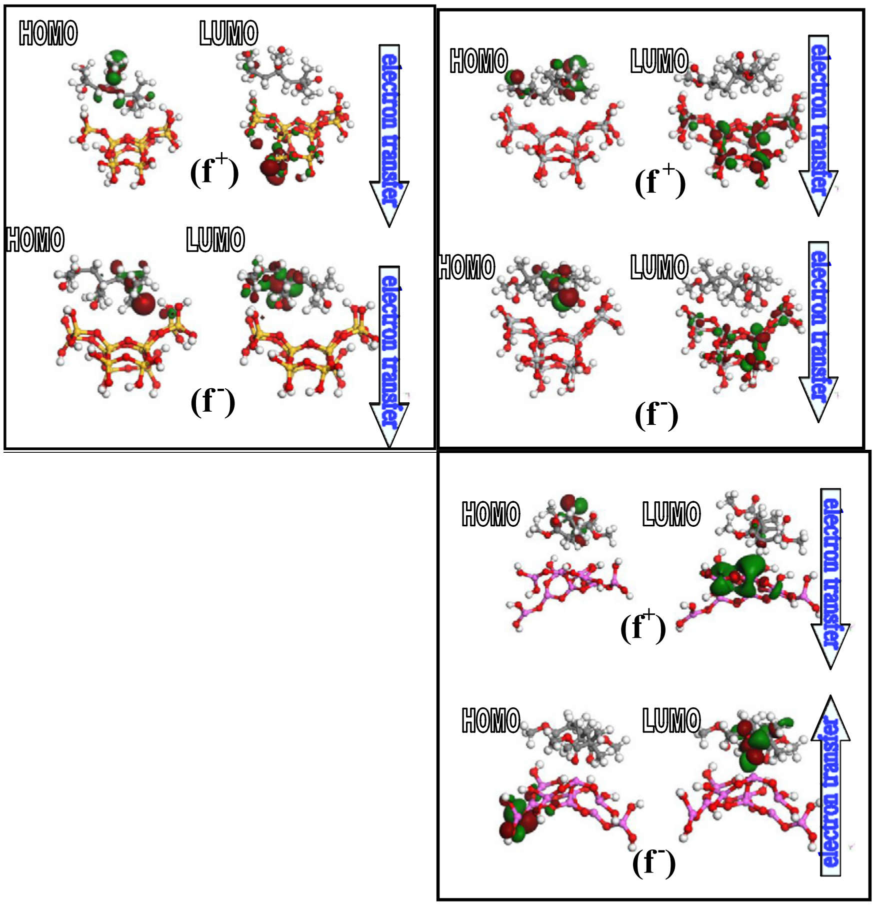

Figure 6. Active electron transfer sites and their orientation dependence as shown by the Fukui functions, f^+ and f^-, for silica, titania, and alumina versus PMMA. Top left: PMMA and silica; top right: PMMA and titania; bottom right: PMMA and alumina.

Table I. Active electron transfer sites and orientation dependence for silica, titania, and alumina versus PMMA.

	Silica		Titania		Alumina	
PMMMA orientation	f^+	f^-	f^+	f^-	f^+	f^-
Charge transfer						
To oxide (eV)	4.61	5.38	2.67	2.89	3.74	4.68
To PMMA (eV)	6.23	5.48	>4.16	>4.21	5.65	3.78

processes will tend to counterbalance, and provided the occurrence of these two orientations in surface collisions is similar, we predict that alumina will not charge well with respect to PMMA. In the next section we will show that these predictions of the net charge are borne out by experiment, and fit the charging data both qualitatively and quantitatively.

In order to develop a predictive model, it is important to understand the different orientations and what chemistry is present at the surfaces. On contact in a charge transfer event when two surfaces collide the collisional orientation defines a complex with a HOMO and a LUMO, and a set of associated excited states for that complex. Charge transfer can occur at that collision, depending on an appropriate distribution of the orbitals: a donor orbital on one surface and an acceptor orbital on the other surface. Thus for charge exchange to occur the appropriate chemical sites must be at the surface and must be in the required orientation for charge transfer. Since there are many different collisions it would be expected that all conformations and chemistries that are expressed at the surface will be sampled at some point, and thus can potentially contribute to the charge. Moreover, of course, the relative contribution of each of these configurations will depend on its probability of occurrence at the surface and any surface morphological effects that might affect the contact frequency. If a particular chemistry or conformation responsible for charge transfer is not present at the surface, due to some preferential orientation of the molecules, then that site would not contribute to charge transfer. Thus preferred configurations at the surface can affect the charge compared to the charge that we would predict from our model, which does not take into account any preferred configurations. We will show an example of the potential importance of a preferred configuration later in the discussion below. Ultimately, the ability of our modeling to fit the data, both qualitatively into a tribo series and quantitatively compared to triboelectric charging parameters and contact potentials, is a test of both the model and these key assumptions.

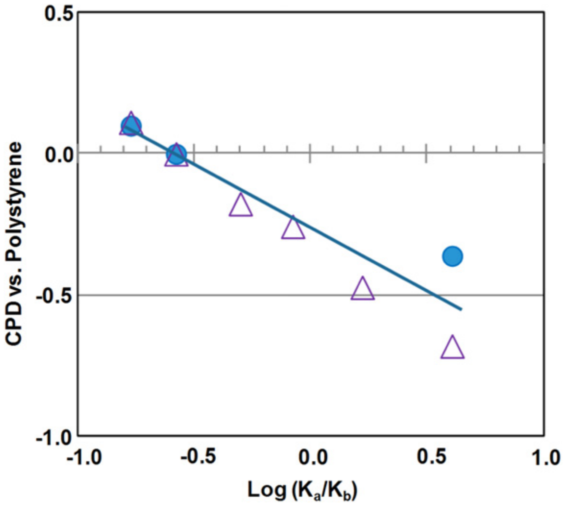

Figure 7. Relationship of chemical potentials to surface acid–base parameters: △ calculated from K_a/K_b and oxide CPD data; ● measured by Yanagida.[32]

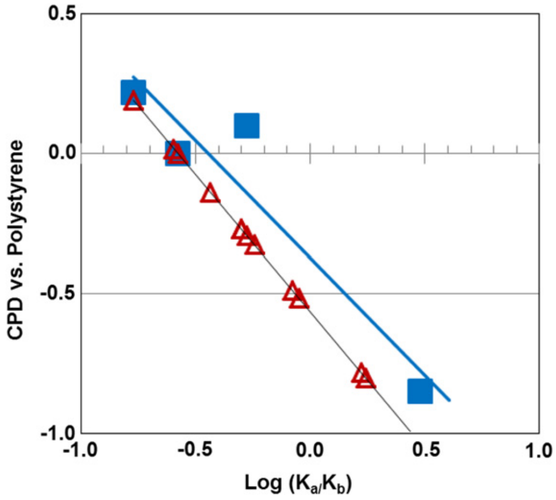

Figure 8. Relationship of chemical potentials to surface acid–base parameters: △ calculated from K_a/K_b and oxide CPD data; ■ measured by Strella.[33]

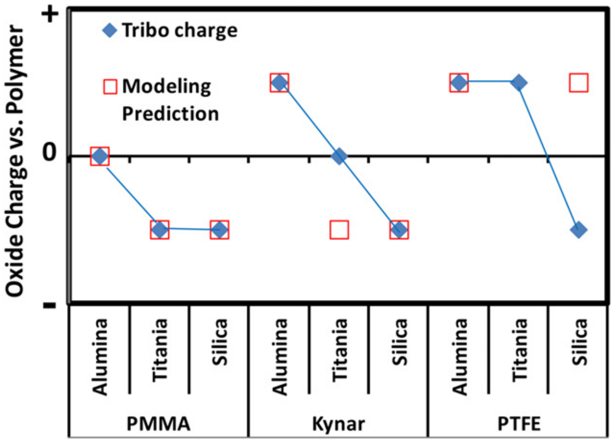

Figure 9. Prediction of direction of charge transfer from DFT modeling and triboelectric charging.

Linking QM modeling to acid–base parameters, contact potentials, and triboelectric charging

We have now established the basis for a QM model as well as the previous acid–base model for electron charge transfer. The next step is to develop quantitative links between the different data sets, the QM modeling data, the surface acid–base data, the contact potential data, and the charge data.

In previous work metal oxide contact potentials were measured[30] and correlated strongly to K_a/K_b values.[3] From that correlation, and published K_a and K_b values,[31] it is possible to predict CPD values. Figure 7 shows CPD values referenced to polystyrene. There are few CPD measurements in the literature for polymers that also have known measured K_a/K_b values. Also, CPD values that are measured by Kelvin potential or UV photoelectron spectroscopy (PES) have the advantage that they are non-contact, which makes them insensitive to the material cross-contamination on contact, as well as the nature of the contact. Indeed, comparison of contact potentials or work functions of insulative materials by contact methods shows little consistency. Yanagida[32] measured work functions at 40% RH by CPD and by UV photoelectron spectroscopy. CPD and K_a/K_b values, which were measured as a function of RH,[30] were interpolated to 40% RH to compare to Yanagida's CPD values. The correlation shown between the predicted CPD from K_a/K_b and the measured CPD from Yanagida in Fig. 7 is reasonable, although data are very limited. The Yanagida data that are fitted are for polystyrene (PS), PMMA, and polyvinylchloride (PVC). It should be pointed out that the actual K_a/K_b values are measured at 0% RH, and thus the extension to 40% RH to predict CPD assumes that the RH sensitivity of the K_a/K_b values and CPD values for the predicted materials is the same as that of the metal oxides, since metal oxides are the only materials here for which we have RH data available. Figure 8 shows a comparison of the predicted CPD from K_a/K_b values to the CPD data collected by Strella[33] using Kelvin potentials at high temperature (to increase conductivity to enable the CPD measurements), and thus with low water content. These values thus are best compared to the CPD predictions of the K_a/K_b values at 0% RH, which is what is shown in Fig. 8. Again the fit is reasonable although again the data are limited. The Strella data fitted are for PMMA, PS, polycarbonate (PC), and PTFE. Overall the quantitative predictions from the acid–base values are supported by the experimental CPD data.

Figure 9 shows the predicted polarity of charge exchange, using DFT to calculate the precursor energy levels, as was done for example in Fig. 6 and Table I, then comparing the energy gaps to determine the lower energy or forward charge transfer direction. The DFT predictions were compared to those measured by mixing powders and measuring a triboelectric charge blow-off. Here we are *qualitatively* predicting the triboelectric series. We do this qualitatively only, because due to the disparate sizes, densities, shapes, and concentrations of the various materials used in the triboelectric blow-off, it was not possible to correct the charge data to account for these factors. Note that in Fig. 9 the data are organized in the direction of the expected triboelectric series based on the K_a/K_b values, so PMMA on the left is predicted to be most positive, PTFE most negative, with Kynar in the middle. Similarly, for the oxide the alumina on the left is most positive, the silica on the right most negative, with titania in the middle. Thus it is generally expected based on the acid–base model that the oxide charge will get progressively more negative from alumina to titania to silica, and similarly that the charge of the additive should get less negative, or more positive, as we progress from PMMA on the left, to Kynar, and then PTFE on the right. As shown in Fig. 9, for the most part both of these general trends are observed: the order of the oxide and of the polymers is mostly as expected, both for measured triboelectric charge and for the QM DFT modeling prediction. For oxides charging with PMMA all three trends match exactly, acid–base expectations, measured charge, and DFT predictions, including the zero charge for alumina with PMMA. Alumina and silica are predicted correctly for charging with Kynar, but titania is predicted to be negative, while no charge exchange was observed. However, titania is predicted to be to the negative side compared to alumina in the Kynar series, which is the observed order—in other words we do predict the triboelectric series, from positive to negative: alumina is more positive than titania. For the Kynar–titania pair the two key conformations were studied, with the Kynar CH bond facing the oxide, or the Kynar CF bond facing the oxide. The CH orientation yields an energy gap preference for electron transfer from Kynar to titania, but does not show a reverse transfer. The CF orientation did not show any appropriate states for electron transfer. Thus for Kynar we were not able to find any states where Kynar was an acceptor, in either configuration. It is not clear whether this is a limitation of the modeling, either in the model for titania or in the model for the oxide. There may be other orientations that enable Kynar as a donor that were not yet explored in the modeling. If there is indeed a missing acceptor state in another orientation that the modeling misses, this could explain the experimental result. Another possibility is that there is a preferential orientation of the Kynar on the surface. If the CH bond is not expressed on the surface, only the CF bond is exposed, then the modeling predicts no charge transfer, as only the CH bond orientation shows possible electron transfer with titania. Again, this would be in agreement with experiment. Of course this preferred orientation would also potentially affect the charging of Kynar with silica and alumina. As it turns out, the modeling for silica and alumina with Kynar in the CF orientation would not change the predicted charge polarity, as both CH and CF orientations lead to a negative silica charge, while the CF orientation dominates the alumina charge. Thus the model and experimental data for Kynar are fully consistent with all the observed oxide charge polarities, if Kynar predominantly exposes CF on the surface. Such an orientational preference in fact should be expected, as the lowest energy configuration would preferentially have the low surface energy CF bond at the surface. For charging with PTFE, alumina is predicted by DFT to be positive as observed, but silica is also predicted to be positive, while the observed charge is negative. Interestingly, as we will show later, the K_a/K_b values predict silica to be positive with respect to PTFE in agreement with the DFT modeling, so here the observed charge seems to be the odd man out. Indeed, PTFE is a difficult material to measure experimentally, as it is very prone to material physical transfer due to its softness, so experimental measurements of charging are known to show polarity reversals.[34] For titania, even inspecting 11 excited states with DFT, no charge transfer was seen; no acceptor or donor was found for PTFE, though higher states might provide transfer opportunities. DFT accuracy suffers too much, however, to attempt to calculate higher excited states. This could indicate that the modeling is missing something for PTFE or titania. This could be because the molecular structure used in the model is too simple and misses some key aspect—this seems more likely for the titania, whose surface chemistry could be much more complicated than modeled, while PTFE is a relatively simple structure and should be well represented by the trimer model used here. It might also be that there is another configuration of the charge transfer complex other than the one studied for PTFE that is important for charge transfer. Overall there is reasonable qualitative agreement between the modeling and the observed triboelectric series, and the expectations of the acid/base model, though more work is needed.

To make a quantitative link between the CPD values, the chemical potentials, and the surface chemistry of the acceptor and donor sites, we can rearrange Eq. (3), writing it in a general form for any two surfaces, A and B,

$$\begin{aligned} CPD &= [(\phi_{b(A)} - \phi_{a(B)}) - (\phi_{b(B)} - \phi_{a(A)})] \\ &= C \cdot \ln[K_a(A)/K_b(A)] - \ln[K_a(B)/K_b(B)], \end{aligned} \tag{7}$$

where C is a constant. The energy difference $[(\phi_{b(A)} - \phi_{a(B)})]$ in Eq. (3) is the energy gap for material A as a donor and material B as an acceptor, while the energy difference in Eq. (3) is the energy gap for material B as the donor and material A as the acceptor. The interrelationships can also be seen from Fig. 1. Also, using Eqs. (3) and (4), the CPD can be expressed in terms of the K_a/K_b values. Thus, if we plot the energy difference, $\Delta E(\text{Donor}) - \Delta E(\text{Acceptor})$, for the polymer with the different metal oxides, as calculated by DFT, which is the calculated CPD, with respect to the measured CPD for the polymer and the same metal oxides, as calculated by the K_a/K_b values, we expect a straight line with intercept of zero (there is no constant term in Eq. (7)). If the energy gap difference is negative, the polymer is a better donor than acceptor for the metal oxides, as is seen for PMMA in Figure 10. If the energy gap difference is positive, the polymer is a better acceptor than donor for the metal oxides, as seen for PTFE in Fig. 10. Similarly, the PMMA–oxide CPD values are negative, for PTFE–oxide positive. The correlation shown in Fig. 10 also passes close to the origin, as it should, although the best fit slope is

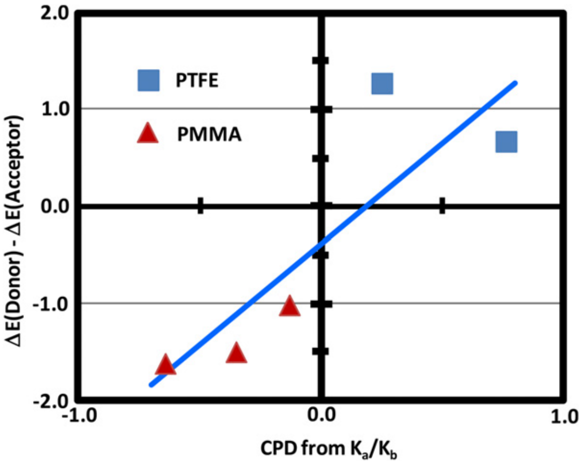

Figure 10. Energy gaps in a precursor complex with the polymer as the donor or acceptor compared to the CPD values of silica, alumina, and titania with PMMA and PTFE.

not exactly 1:1 as would be expected, although given the limit data and experimental uncertainties, the fit is not inconsistent with a 1:1 slope. Overall, it is an encouraging start to developing a quantitative model.

As a final check of the quantitative model for DFT and the acid–base model, we can compare the individual DFT calculated donor–acceptor gaps for PMMA and PTFE with the metal oxide additives to the CPD values calculated from the K_a and K_b values. Referring to Fig. 1, the donor–acceptor energy gaps are

$$E_g(A,B) = \phi_b(A) - \phi_a(B);\ E_{g(B,A)} = \phi_b(B) - \phi_a(A). \quad (8)$$

Here we are again writing the equation for the two general surfaces A and B, and where the two gaps represent the two possibilities for charge transfer, $E_g(A,B)$ where A is the donor, $E_g(B,A)$ where B is the donor. Now ϕ_a increases with $\ln K_a$ and ϕ_b increases with $-\ln K_b$, as shown by Eqs. (13) and (14) in reference 3 (Part 1). Using these relationships, Eq. (8) becomes

$$\begin{aligned} E_g(A,B) &= \ln[K_a(A)K_b(B)]; \\ E_g(A,B) &= \ln[K_a(B)K_b(A)]. \end{aligned} \quad (9)$$

Figure 11 shows the plot of Eq. (9) for the two polymers PMMA and PTFE as either donor or acceptor to the metal oxide additives, silica, titania, and alumina. The correlation is reasonable, considering that it is a comparison of the predictions of the DFT model of the energy gaps and the predictions of the K_a/K_b model of the CPD differences. The plot does indeed show that the energy gaps between the donor and acceptor follow the expected trend, the larger K_a (the better the acceptor) and K_b (the better the donor) the smaller the energy gap. PTFE as a donor appears to be showing more variation than as an acceptor, or than the PMMA. PTFE is an excellent acceptor, but a terrible donor, so it may be that it is just difficult to predict the very weak donation capacity in this case. Again, this is good support of the DFT and acid–base model for the donor and acceptor states in polymers and metal oxides.

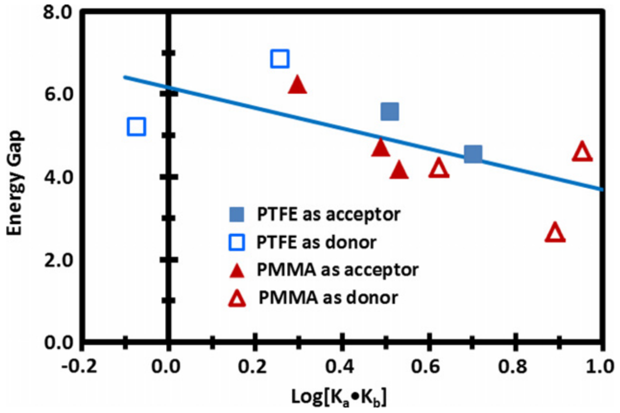

Figure 11. Energy gaps in the precursor complex to triboelectric charging of silica, alumina, and titania versus PMMA for forward and reverse gaps.

CONCLUSIONS

Progress has been made in the integration of chemistry and physics in a reasonably complete model of charge transfer in insulators, coupling both the theory and experiment. Both DFT QM modeling and observed IGC acid–base parameters have enabled new understanding of the key elements of electronic charge exchange in insulators. The key elements of that integrated model are as follows.

(1) The high density of surface states model.
(2) The surface states are Lewis base electron donors and acid acceptors.
(3) Charge transfer is enabled by a precursor charge transfer complex of the two materials in contact.
(4) The Lewis base sites are associated with the HOMO and its excited states of the precursor charge transfer complex.
(5) The Lewis acid sites are associated with the LUMO and its excited states of the precursor charge complex.
(6) Both materials can potentially act as both a donor and an acceptor; thus charge transfer is bidirectional, and the net charge transferred is determined by both processes.
(7) The orientation of the molecules at the interface between the two surfaces is critical to the ability to transfer charge and to the magnitude of the electron transfer gaps.
(8) The orientation of the molecular dipoles at the surface is critical to the electron transfer gaps.
(9) The energy required for the electron transfer is too large to be supplied by thermal energy and is proposed to be supplied by the collisional energy on contact of the two surfaces.

DFT QM modeling of precursor charge transfer complexes calculates the energy gaps for forward and reverse charge transfer processes in the bidirectional model, which shows promise to predict the triboelectric series for polymers and metal oxides, and to predict quantitative contact potential differences, which are in turn predicted by the material's surface K_a/K_b acid–base parameters. This study does not rule out a contribution of ionic charge transfer in insulators, though it does show that for the metal oxides and polymers studied here an electron transfer process is fully consistent and appears to be sufficient to describe the salient features of the charge transfer.

REFERENCES

[1] E. J. Gutman and G. C. Hartmann, "Triboelectric properties of two component developers for xerography," J. Imaging Sci. Technol. **36**, 335–349 (1992); E. J. Gutman and G. C. Hartmann, "The role of the electric field in triboelectric charging of two component xerographic developers," J. Imaging Sci. Technol. **39**, 285–294 (1985).

[2] L. B. Schein, J. Imaging Sci. Technol. **37**, 1 (1993); J. H. Anderson, "Surface state analysis of tribocharging data: effects of carbon blacks," J. Imaging Sci. Technol. **44**, 129–131 (2000); J. H. Anderson, "A method for quantitatively determining triboelectric series and its applications in electrophotography," J. Imaging Sci. Technol. **44**, 534–543 (2000).

[3] R. P. N. Veregin, M. N. V. McDougall, M. S. Hawkins, C. Vong, V. Skorokhod, and H. P. Schreiber, "A bidirectional acid–base charging model for triboelectrification: Part 1. Theory," J. Imaging Sci. Technol. **50**, 282–287 (2006); R. P. N. Veregin, M. N. V. McDougall, M. S. Hawkins, C. Vong, V. Skorokhod, and H. P. Schreiber, "A bidirectional acid–base charging model for Triboelectrification: Part II. Experimental verification by Inverse Gas Chromatography and charging of metal oxides," J. Imaging Sci. Technol. **50**, 288–293 (2006).

[4] E. Nikitina, H. Barthel, and M. Heinemann, "Electron transfer in electrical tribocharging using a quantum chemical approach," J. Imaging Sci. Technol. **53**, 040503-1–40503-9 (2009).

[5] *Dmol3*, release 4.2 (Accelrys, Inc., San Diego, CA, 2001).

[6] S. R. Stoyanov, S. Gusarov, S. M. Kuznicki, and A. Kovalenko, "Theoretical modelingof zeolite nanoparticle surface acidity for heavy oil upgrading," J. Phys. Chem. C. **112**, 6794–6810 (2008).

[7] J. P. Perdew, in *Electronic Structure of Solids '91*, edited by P. Ziesche and P. H. Eschrig, (Akademie Verlag, Berlin, 1991), p. 11.

[8] C. Lo and B. L. Trout, "Density-functional theory characterization of acid sites in chabazite," J. Catal. **227**, 77–89 (2004).

[9] F. Pascale, P. Ugliengo, B. Civalleri, R. Orlando, P. D'Arco, and R. Dovesi, "Hydrogarnet defect in chabazite and sodalite zeolites: a periodic Hartree–Fock and B3-LYP study," J. Chem. Phys. **117**, 5337–5346 (2002).

[10] B. J. Delley, "An all-electron numerical method for solving the local density functional for polyatomic molecules," Chem. Phys. **92**, 508–517 (1990).

[11] B. J. Delley, "From molecules to solids with the DMol3 approach," Chem. Phys. **113**, 7756–7764 (2000).

[12] R. P. N. Veregin, C. P. Tripp, M. N. V. McDougall, and D. Osmond, "The role of water in the triboelectric charging of alkylchlorosilane-treated silicas as toner surface additives," J. Imaging. Sci. Technol. **39**, 429–432 (1995).

[13] S. Leonardelli, L. Facchini, C. Fretigny, P. Tougne, and A. P. Legrand, "Silicon-29 NMR study of silica," J. Am. Chem. Soc. **114**, 6412–6418 (1992).

[14] F. Vigné-Maeder and P. Sautet, "Theoretical study of hydroxylated and dehydroxylated surfaces of a cristobalite model of silica," J. Phys. Chem. B. **101**, 8107–8203 (1997).

[15] S. Iarlori, D. Ceresoli, M. Bernasconi, D. Donadio, and M. Parrinello, "Dehydroxylation and silanization of the surfaces of β-cristobalite silica: an ab initio simulation," J. Phys. Chem. B. **105**, 8007–8013 (2001).

[16] I.-S. Chuang and G. E. Maciel, "A detailed model of local structure and silanol hydrogen bonding of silica gel surfaces," J. Phys. Chem. B. **101**, 3052–3064 (1997).

[17] I.-S. Chuang and G. E. Maciel, "Probing hydrogen bonding and the local environment of silanols on silica surfaces via nuclear spin cross polarization dynamics," J. Am. Chem. Soc. **118**, 401–406 (1996).

[18] A. P. Legrand, *The Surface Properties of Silica* (Wiley, New York, 1998), p. 2.

[19] *Highly Dispersed Metal Oxides Produced by the Aerosil®Process*, Degussa Technical Bulletin Pigments, 56, 9–13.

[20] L.-H. Lee, "Relevance of the density-functional theory to acid–base interactions and adhesion in solids," J. Adhesion. Sci. Technol. **5**, 71–92 (1991).

[21] R. Veregin, M. McDougall, M. Hawkins, C. Vong, V. Skorokhod, and H. Schreiber, "A bidirectional acid–base charging model for triboelectrification: experimental verification by Inverse Gas Chromatography and xerographic charging of toner and carrier," *Proc. IS&T NIP24: Int'l Conf. on Digital Printing Technol. and Digital Fabrication* (IS&T, Springfield, VA, 2008), pp. 30–33.

[22] R. Veregin, M. McDougall, M. Hawkins, C. Vong, and V. Skorokhod, "Understanding the influence of surface acid and base properties and water on work functions and triboelectric charging using Inverse Gas Chromatography," presentation given at *Proc. IS&T NIP22: Int'l. Conf. on Digital Printing Technol.* (IS&T, Springfield, VA, 2006).

[23] S. R. Leadly and J. F. Watts, "The use of monochromated XPS to evaluate acid–base interactions at the PMMA/oxidized metal interface," J. Adhesion **60**, 175–196 (1997).

[24] J. J. Hopfield, "Electron transfer between biological molecules by thermally activated tunneling," Proc. Natl. Acad. Sci. USA **71**, 3640–3644 (1974).

[25] Alpha Labs Inc., *The Triboelectric Series*, web site: http://www.trifield.com/content/tribo-electric-series/, accessed November 2012.

[26] W. R. Harper, *Contact and Frictional Electrification* (Oxford University Press, London, 1967), p. 58.

[27] J. M. Wells and S. A. McLuckey, "Collision-induced dissociation (CID) of peptides and proteins," Meth. Enzymol. **402**, 148–85 (2005); L. Sleno and D. A. Volmer, "Ion activation methods for tandem mass spectrometry," J. Mass Spectrom. **39**, 1091–112 (2004).

[28] M. Mabud, "Surface-induced dissociation of molecular ions," Int. J. Mass Spectrom. Ion Process. **67**, 285 (1985); V. Grill, "Collisions of ions with surfaces at chemically relevant energies: instrumentation and phenomena," Rev. Sci. Instrum. **72**, 3149–3179 (2001); A. E. Blackwell, E. D. Dodds, V. Bandarian, and V. H. Wysocki, "Revealing the quaternary structure of a heterogeneous noncovalent protein complex through surface-induced dissociation," Anal. Chem. **83**, 2862–2865 (2011).

[29] P. W. Ayers, W. Yang, and L. J. Bartolotti, "Fukui Function," *Chemical Reactivity Theory: A Density Functional View*, P. K. Chattaraj, Ed. (CRC Press, Boca Raton, FL, 2009), pp. 255–267.

[30] R. P. N. Veregin, D. Powell, C. P. Tripp, M. N. V. McDougall, and M. Mahon, "Kelvin potential measurement of insulative particles.1. Mechanism of metal oxide triboelectric charging and relative humidity sensitivity," J. Imaging Sci. Technol **41**, 192–196 (1997).

[31] H. Liang, R. Xu, B. D. Favis, and H. P. Schreiber, "Interfacial tension and acid–base approaches to polymer interactions," J. Poly. Sci. B: Polymer Physics **38**, 2096–2104 (2000); J. Lara and H. P. Schreiber, J. Coatings Technol. **63**, 81–90 (1991); H. P. Schreiber, "Specific interactions and contact angle measurements on polymer solids," J. Adhesion **37**, 51–61 (1992); U. Panzer and H. P. Schreiber, "On the evaluation of surface interactions by inverse gas chromatography," Macromolecules **25**, 3633–3637 (1992); F. Thielmann and D. Burnett, "Determination of carbon fibre-polymer interactions by inverse gas chromatography," *American Carbon Society Proc. 2004 Carbon Conference*, M048; H. P. Schreiber, PTFE acid–base values by IGC, private communication.

[32] K. Yanagida, O. Okada, and K. Oka, "Low-Energy Electronic States Related to Contact Electrification of Pendant-Group Polymers: Photoemission and Contact Potential Difference Measurement," Jpn. J. Appl. Phys. **32**, 5603–5610 (1993).

[33] S. Strella and see D. A. Seanor, in *Electrical Properties of Polymers*, edited by A. D. Jenkins, Polymer Science (North-Holland, Amsterdam, 1972), Vol. 2, p. 39.

[34] H. T. Baytekin, B. Baytekin, J. T. Incorvati, and B. A. Grzybowski, "Material transfer and polarity reversal in contact charging," Angew. Chem. Int. Ed. **51**, 4843–4847 (2012).